JOURNAL OF MATERIALS SCIENCE **34** (1999) 329–336

Effect of elastic interaction energy on coarsening of γ' precipitates in a mechanically alloyed ODS Ni-base superalloy

HO J. RYU, SOON H. HONG
Department of Materials Science and Engineering, Korea Advanced Institute of Science and Technology, 373-1 Kusung-dong, Yusung-gu, Taejon, 305-701, Korea
E-mail: shhong@sorak.kaist.ac.kr

J. WEBER, J. H. TUNDERMANN
Inco Alloys International, Inc. P.O.Box 1958, Huntington, WV 25720, USA

The coarsening behavior of γ' precipitates with a uniform size distribution and with a bimodal size distribution in a mechanically alloyed ODS Ni-base superalloy were investigated to clarify the effect of elastic interaction energy on the coarsening behavior of γ' precipitates. The coarsening rate decreased with increasing size of γ' precipitates with a uniform size distribution, contrary to the classical LSW theory, and the coarsening behavior of γ' precipitates with a bimodal size distribution exhibited Ostwald ripening in which the larger precipitates grow at the expense of smaller precipitates. The driving force for coarsening of γ' precipitates was analyzed based on the two-particle model, considering the effect of elastic interaction energy in addition to the effect of interfacial energy. The contribution of elastic interaction energy on the total energy was found to increase with increasing size of precipitates, and the decelerated coarsening of γ' precipitates was attributed to the decrease in the driving force for coarsening with increasing size of precipitates.

1. Introduction

Ni-base superalloys have been widely used for high temperature applications such as turbine blades, turbine disks and turbine vanes in jet engines and industrial gas turbine engines [1, 2]. The excellent mechanical properties of Ni-base superalloys at elevated temperature are mainly due to the high volume fraction of γ' precipitates of $L1_2$ ordered structure, which are stable at high temperature. Since the deformation behavior of Ni-base superalloys is sensitively affected by the size of γ' precipitates, the coarsening behavior of γ' precipitates in Ni-base superalloys during high temperature exposure has been extensively investigated [3–5]. The coarsening behavior of γ' precipitates in Ni-base superalloys is known as Ostwald ripening, in which the larger precipitates grow at the expense of smaller precipitates in order to reduce the total interfacial energy while maintaining a constant volume fraction of the precipitates. The classical theory that describes the Ostwald ripening of precipitates is known as the LSW theory [6, 7]. According to the LSW theory, the cube of the average precipitate size, $r(t)^3$, depends linearly on ageing time, t. Recently, the classical LSW theory has been modified in order to consider the effect of the precipitates volume fraction on the coarsening behavior [8–11].

However, the characteristic phenomena in the coarsening behavior of γ' precipitates of Ni-base superalloys, such as splitting [12], alignment [13] and decelerated coarsening [14–16] of precipitates cannot be explained by the classical coarsening theories. These characteristic coarsening phenomena of γ' precipitates in Ni-base superalloys are attributed to the effects of lattice misfit between the γ' precipitates and the γ matrix. The lattice misfit between the γ' precipitates and the γ' matrix induces the elastic strain fields around the γ' precipitates. When the inter-particle spacing of the γ' precipitates is small enough, the elastic strain fields overlap and cause a change in the total elastic energy. The change in the total elastic energy due to the interaction of elastic strain fields around the precipitates is known as the elastic interaction energy [17–19].

Several researchers have observed the decelerated coarsening behavior of γ' precipitates in Ni-base alloys [14–16, 20–23]. Most of the researcher [22, 23] explained the decelerated coarsening behavior by using the concepts of bifurcation theory, proposed by Johnson [24], based on the two-particle model shown schematically in Fig. 1, where r_1 and r_2 are the radii of the particles and L is the inter-particle spacing. The three-dimensional bifurcation diagram showing the change of total energy plotted against a parameter corresponding to the relative size change of two particles, $(r_1 - r_2)/(r_1 + r_2)$, and the inter-particle spacing, L, is plotted in Fig. 2. The bifurcation diagram exhibits two distinct regions: region I in which the minimization of total

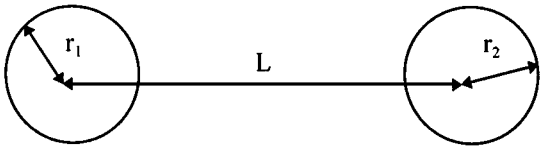

Figure 1 Schematic diagram of the two particle model used in the bifurcation theory. r_1 and r_2 are the radii of the particles and L is the inter-particle spacing [24].

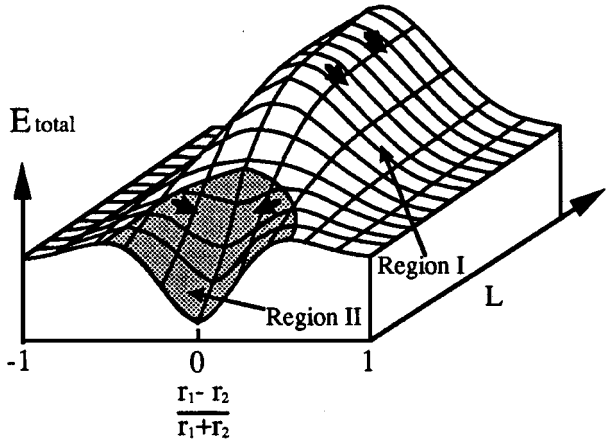

Figure 2 Three-dimensional bifurcation diagram composed of region I, in which the Ostwald ripening occurs, and region II, in which the inverse coarsening occurs [20].

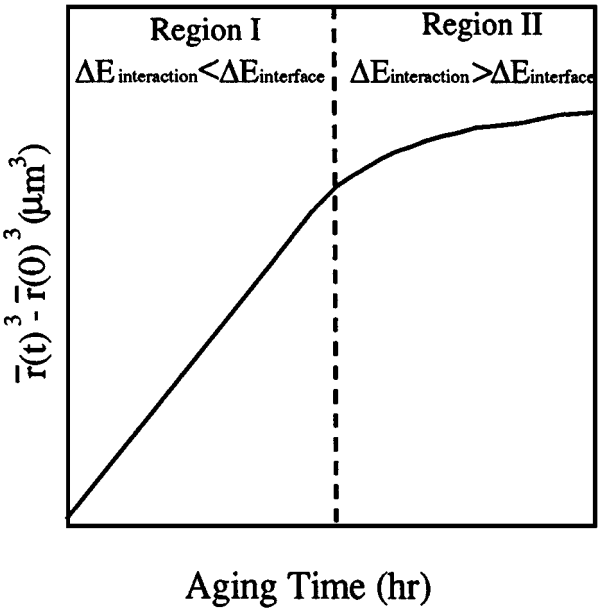

Figure 3 Schematic illustration showing the change in coarsening rate with ageing time [23].

energy is achieved when $r_1 \gg r_2$ or $r_2 \gg r_1$, and region II in which the minimization of total energy is achieved when $r_1 = r_2$. The coarsening rate is maintained constant with the ageing time in region I, satisfying the LSW theory, where the contribution of the elastic interaction energy to the change of total free energy is smaller than the contribution of the interfacial energy. On the other hand, the smaller precipitates can grow at the expense of the larger precipitates and thus show an inverse coarsening behavior in region II, where the contribution of elastic interaction energy to the change of total energy is larger than the contribution of the interfacial energy. Decelerated coarsening behavior has been attributed to the inverse coarsening behavior of γ' precipitates in region II, as plotted schematically in Fig. 3 [22]. The inverse coarsening behavior, however, has not been studied systematically yet in alloys with elastically interacting precipitates [25–28].

In this study, the decelerated coarsening behavior of γ' precipitates in a mechanically alloyed ODS Ni-base superalloy was investigated to clarify the effect of the elastic interaction energy on the coarsening behavior of γ' precipitates. The variation of the driving force in the coarsening of γ' precipitates was analyzed considering the contribution of the elastic interaction energy to the total energy with increasing precipitate size based on the theoretical two-particle model.

2. Experimental procedure

The chemical composition (wt%) of the mechanically alloyed ODS Ni-base superalloy investigated in this study is Ni–5Co–8Cr–5.5Al–1Ti–6Ta–1Mo–8W–2Re–0.03B–0.01Zr–0.9Y_2O_3. The powders were mechanically alloyed for 30 h in a high energy attritor. The mechanically alloyed powders were sealed in mild steel cans and hot extruded into bars of 19 mm diameter with an extrusion ratio of 18 : 1 at a temperature of 1177 °C. The hot extruded bars were zone annealed to form a coarse elongated grain structure by moving a furnace along the extruded bars at a constant speed of 65 mm hr^{-1} and a maximum hot zone temperature of 1300 °C. The zone-annealed bars were solution treated at 1270 °C for 30 min or 1210 °C for 30 min, then air-cooled to room temperature to obtain a uniform size distribution or a bimodal size distribution, respectively. The ageing treatments were carried out at 950 °C for various ageing time from 2 to 200 h to control the size of the γ' precipitates. The lattice misfit between the γ' precipitates and the γ matrix at the ageing temperature of 950 °C was measured by X-ray diffraction (XRD) analysis using CuK_α radiation at room temperature, 950 °C and 1050 °C. Scanning electron micrographs (SEM) were observed to measure the average sizes of the cuboidal γ' precipitates after electroytic etching of the polished surface with a 10% nitric acid and 5% acetic acid solution. Transmission electron microscopy (TEM) specimens were electropolished in a Struers Tenupole twin jet electropolisher operating at 30 V in a 9 : 1 mixture of ethanol and perchloric acid at −50 °C. The elastic interaction energy and the interfacial energy were calculated using the data listed in Table I.

3. Results and discussion

The microstructures of an ODS Ni-base superalloy after zone annealing are shown in Fig. 4. The grain structure is coarse and elongated along the extrusion direction as shown in Fig. 4a due to the secondary recrystallization of fine grains in the extruded bar during the zone annealing. The average aspect ratio of the elongated grains was measured to be about 5 : 1. The shape of the

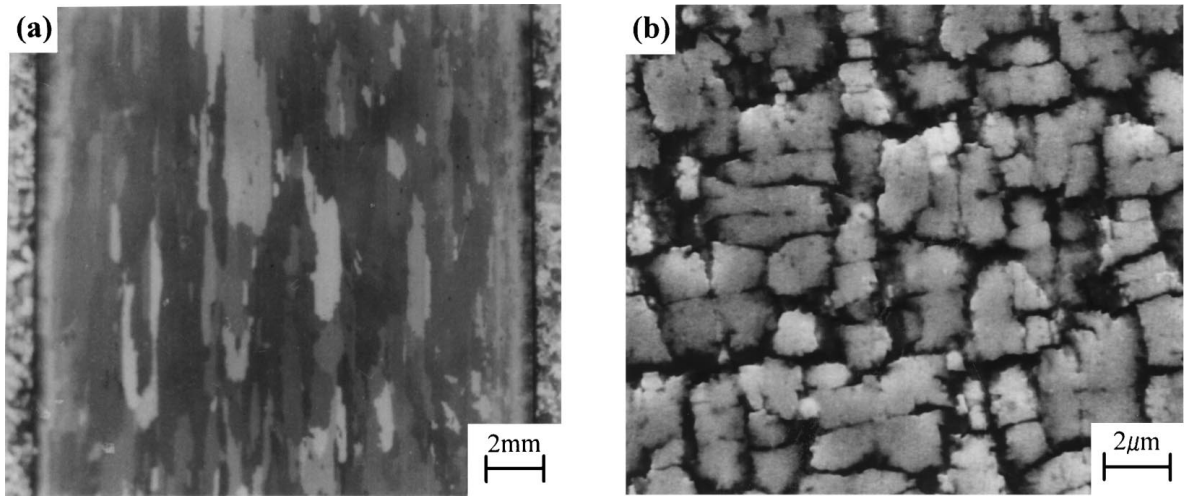

Figure 4 SEM micrograph showing (a) the grain structure and (b) the shape of γ' precipitates of ODS Ni-base superalloy specimen after zone annealing at 1300 °C with traveling speed of 65 mm h^{-1}.

TABLE I Numerical values used for the calculation of elastic interaction energy and interfacial energy in Ni-base superalloys [20, 22]

Elastic constants of the matrix	$C_{11} = 112\,400$ MN m^{-2}
	$C_{12} = 62\,700$ MN m^{-2}
	$C_{44} = 56\,900$ MN m^{-2}
Elastic constants of the precipitates	$C_{11} = 166\,600$ MN m^{-2}
	$C_{12} = 106\,500$ MN m^{-2}
	$C_{44} = 99\,200$ MN m^{-2}
Lattice misfit	$\delta = -0.002$
Interfacial energy density	$\gamma_0 = 0.0142$ J m^{-2}
Precipitates volume fraction	$f = 0.65$
Inter-particle distance	$L = (V/f)^{\frac{1}{3}}$

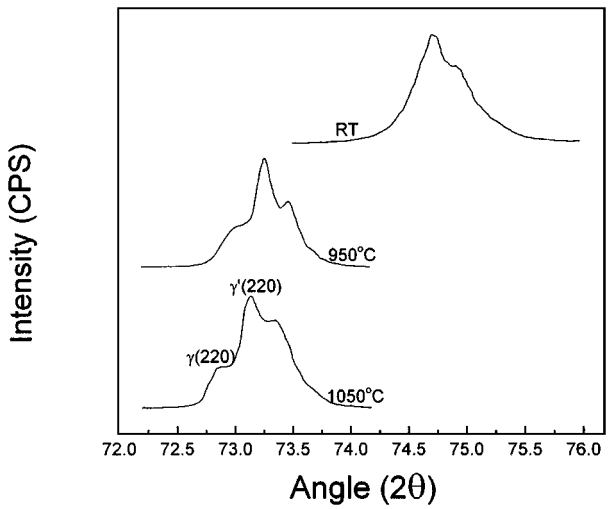

Figure 5 X-ray diffraction showing the lattice misfit between the γ' precipitates and the matrix in ODS Ni-base superalloy at room temperature, 950 °C and 1050 °C.

γ' precipitates in Ni-base superalloys after zone annealing was observed to be dendritic octets, as shown in Fig. 4b. The volume fraction of the γ' precipitates was measured to be about 65% by the point-counting method and their size was measured to be about 1–2 μm. Fig. 5 shows the diffraction intensity of the (2 2 0) peaks from the γ' precipitates and γ matrix at room temperature, 950 °C and 1050 °C. The lattice parameters of the γ' precipitates ($a_{\gamma'}$) and the γ matrix (a_γ) at 950 °C, which was the ageing temperature used in this study, were measured, and the lattice misfit, δ, between the γ' precipitates and the γ matrix at 950 °C was calculated as -0.002 according to

$$\delta = \frac{a_{\gamma'} - a_\gamma}{a_\gamma} \quad (1)$$

Because the solvus temperature of γ' precipitates in a mechanically alloyed Ni-base superalloy in this study was known to be 1260 °C [29], the size distribution of the γ' precipitates showed a uniform size distribution after solution treatment at 1270 °C and a bimodal size distribution after solution treatment at 1210 °C, as shown in Fig. 6. The bimodal size distribution after solution treatment at 1210 °C was due to the formation undissolved coarse γ' precipitates during solution treatment and of newly nucleated fine γ' precipitates during cooling to room temperature.

The γ' precipitates with a uniform size distribution coarsened with increasing ageing time, as shown in Fig. 7. The variation of the cube of average γ' precipitate size against ageing time at 950 °C was plotted, as shown in Fig. 8. The cube of the average γ' precipitate size did not increase linearly with increasing ageing time, and the non-linear coarsening behavior could not be explained by the conventional coarsening theory. The coarsening behavior of γ' precipitates shown in Fig. 8 indicates that the coarsening rate decreased gradually with increasing ageing time. While the mean coarsening rate was about 5.0×10^{-5} mm^3 h^{-1} at the initial stage of ageing, the mean coarsening rate decreased to 1.4×10^{-5} mm^3 h^{-1} at the final stage after 200 h ageing time.

The coarsening behavior of γ' precipitates with a bimodal size distribution was observed in order to investigate the theoretically expected inverse coarsening behavior, because the decelerated coarsening behavior of elastically interacting precipitates has been attributed to inverse coarsening behavior in which smaller precipitates coarsen at the expense of larger precipitates [22]. The coarsening behavior of γ' precipitates with a bimodal size distribution, however, exhibited typical

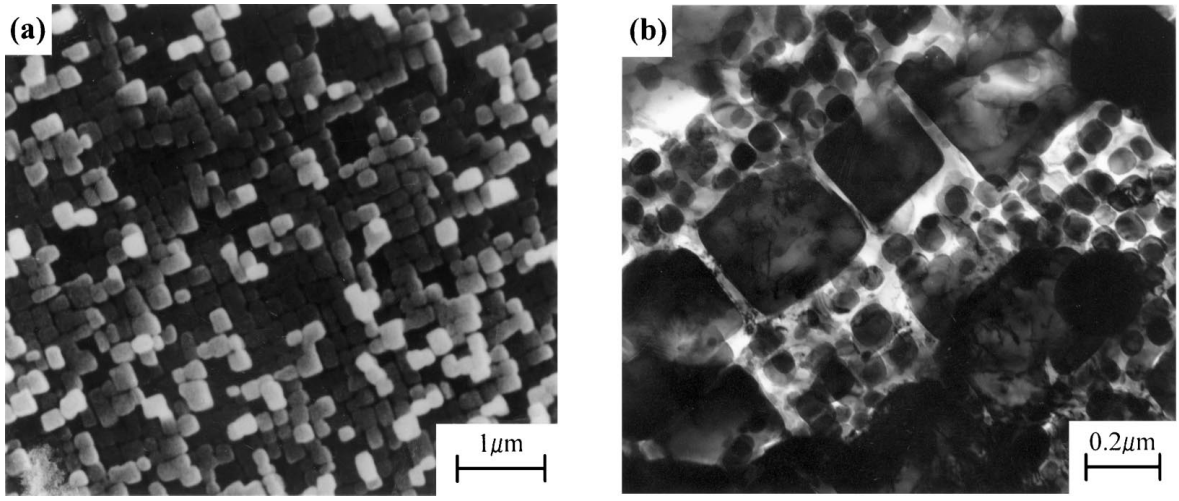

Figure 6 (a) SEM micrograph showing the uniform size distribution of γ' precipitates after solution treatment at 1270 °C for 30 min, and (b) TEM micrograph showing the bimodal size distribution of γ' precipitates after solution treatment at 1210 °C for 30 min.

Ostwald ripening, as shown in Fig. 9, without showing inverse coarsening behavior. The larger precipitates shown in Fig. 9a coarsened at the expense of the smaller precipitates, and the latter almost disappeared after 48 h ageing treatment at 950 °C, as shown in Fig. 9b. This result shows that the decelerated coarsening behavior of elastically interacting precipitates may occur without inverse coarsening behavior, contrary to previous explanations. Therefore, the decelerated coarsening behavior of γ' precipitates needs to be explained without the concept of the inverse coarsening behavior of elastically interacting precipitates.

In order to analyze the decelerated coarsening behavior of γ' precipitates, the change in the total free energy (ΔE_{total}), which consisted of the change in the interfacial energy (ΔE_{surf}) and the change in the elastic interaction energy (ΔE_{int}), was calculated by using the two-particle model used in the bifurcation theory [24]. The elastic interaction energy between the two particles was obtained from the equation of Yamauchi and de Fontaine [30] expressed as follows

$$E_{\text{int}} = \frac{V_1 V_2}{16\pi^2 L^3} \int_0^{2\pi} \left[\frac{\partial^2}{\partial \theta^2} W(\mathbf{n}) \right]_{\theta=\pi/2} d\psi \qquad (2)$$

where V_1 and V_2 are the volumes of the two particles, L is the inter-particle spacing θ and ψ define the direction of the unit vector **n** and W**(n)** is a function related to the elastic strain energy as follows

$$W(\mathbf{n}) = A_j (G^{-1})_{jk} A_k \qquad (3a)$$

where

$$A_j = C_{jklm} n_k \eta_{lm}$$
$$G_{jk} = C_{jklm} n_l n_m \qquad (3b)$$

in which $(G^{-1})_{jk}$ is the Green's tensor, η_{lm} is the equivalent eigenstrain, C_{jklm} is the elastic stiffness constant [31].

The numerical values for the calculation of the elastic interaction energy and the interfacial energy in the two-particle model are listed in Table I, and the calculated elastic interaction energy using the data is expressed as

$$E_{\text{int}} = -1.55 \times 10^5 V^2 / L^3 = -1.55 \times 10^5 \phi V = -BV \qquad (4)$$

where ϕ is the volume fraction of the particle, V is the particle volume and B is a constant. The interfacial energy for the two-particle model is expressed simply as

$$E_{\text{surf}} = \gamma_s A \qquad (5)$$

where γ_s is the interfacial energy density and A is the total interfacial area. The particle shape is assumed to be spherical for this simple calculation.

The total energy is plotted against the parameter R, which is $(r_1 - r_2)/(r_1 + r_2)$, and the inter-particle spacing, L, in Fig. 10. The values of total energy were normalized by the total energy at $r_1 = r_2$ to show how the gradient of energy changes with increasing particle size. When there is no contribution from the elastic interaction energy, the gradient of energy does not change with increasing particle size from 0.16 μm to 0.32 μm, as shown in Fig. 10a and b. When there is a contribution from the elastic interaction energy, the gradient of energy changes apparently with increasing particle size from 0.16 μm to 0.32 μm, as shown in Fig. 10c and d. The variation of the gradient of total energy shown in Fig. 10c and d reveals the effect of the elastic interaction energy decrease energy difference between initial stage and final stage of coarsening. This calculated result indicates that there is a variation of the driving force in coarsening with increasing particle size when the elastic interaction energy has an effect.

To analyze the variation of the driving force in coarsening, the effect of the elastic interaction energy on the solubility of the precipitates was studied. When there is no elastic interaction energy, the change in the total free energy is given by

$$dE = dE_{\text{surf}} = \gamma_s dA \qquad (6)$$

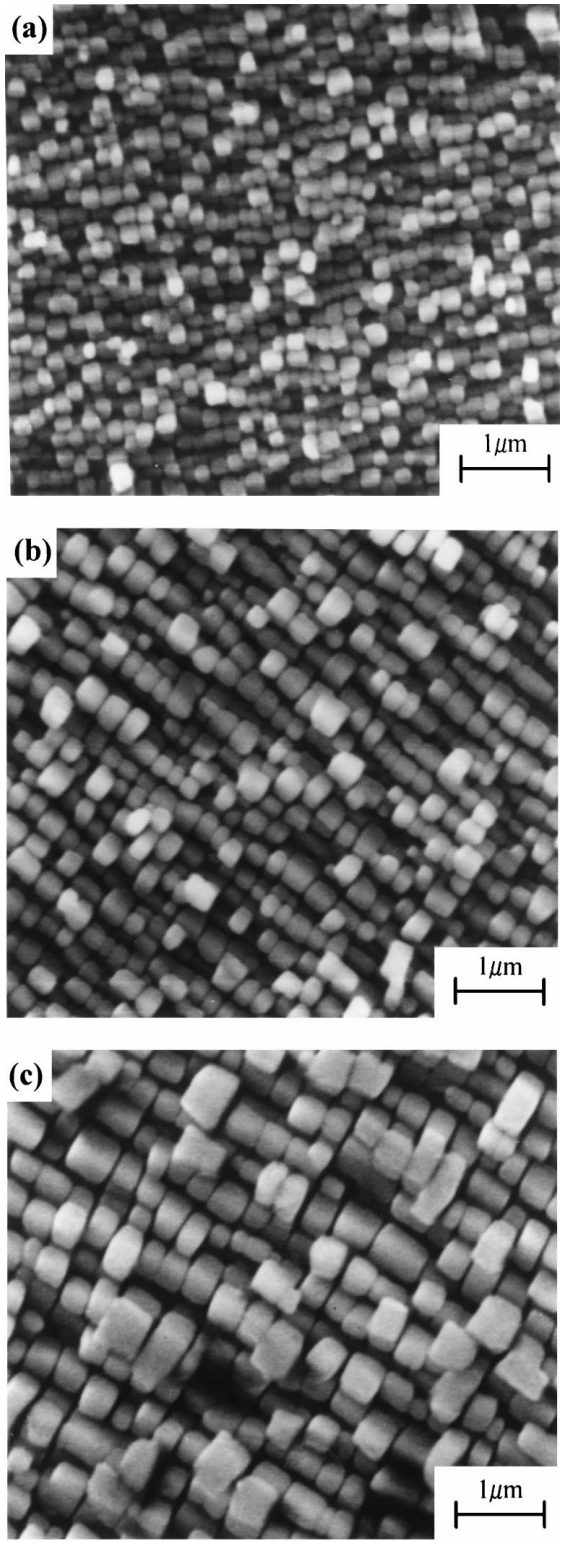

Figure 7 SEM micrograph showing the coarsening of γ' precipitates with ageing time at 950 °C for (a) 2 h, (b) 30 h and (c) 120 h.

When there is an elastic interaction energy, the change in the total free energy is

$$dE = dE_{\text{surf}} + dE_{\text{int}} = \gamma_s dA - BdV \qquad (7)$$

and the driving force for coarsening is expressed as

$$\Delta G_s = dE/dn \qquad (8)$$

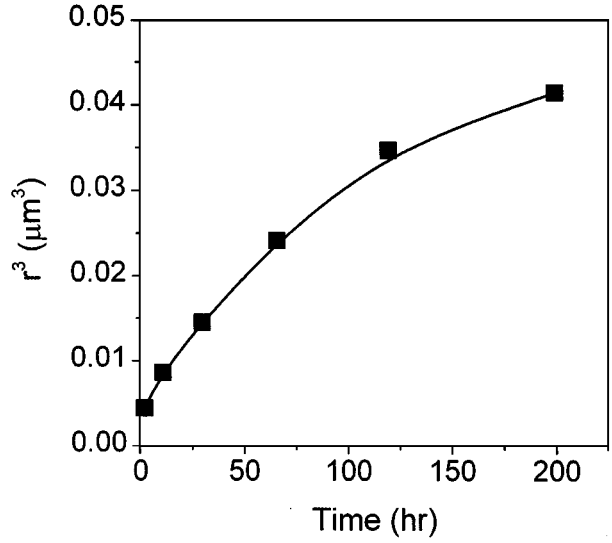

Figure 8 The variation of the cube of average γ' precipitates in ODS Ni-base superalloy with ageing time at 950 °C.

where $n = 4\pi r^3/3V_m$ When there is no elastic interaction energy, the driving force of coarsening is

$$\Delta G_s = \frac{2\gamma_s V_m}{r} \qquad (9)$$

and when there is an elastic interaction energy, the driving force of coarsening is as follows

$$\Delta G_i = \frac{2\gamma_s V_m}{r} - BV_m \qquad (10)$$

The difference between Equation 9 and 10 shows that the elastic interaction energy affects the driving force of coarsening of precipitates, and the contribution of the effect of the elastic interaction energy becames more important with increasing particle size.

The coarsening rate, k_{MLSW}, in the conventional LSW theory is given by

$$k_{\text{MLSW}} = \frac{8}{9}\frac{DC_e\gamma_s V_m^2 f(\phi)}{RT} \qquad (11)$$

where V_m is molar volume, D is diffusivity, C_e is equilibrium concentration of precipitates, γ_s is interfacial energy density and $f(\phi)$ is defined as $k(\phi)/k(0)$, which is the ratio of the coarsening rate with a finite volume fraction of precipitates, ϕ, to the coarsening rate with a zero volume fraction. According to Ardell [32], $f(\phi)$ is in the range 1–4 and the coarsening rate is known to be maintained constant during the coarsening of precipitates.

The effect of the driving force obtained in Equations 9 and 10 is included in terms of solubility in the coarsening rate. The solubility of a particle of radius r in the matrix is referred to as the Gibbs–Thomson equation as follows

$$C_r = C_e \exp\left(\frac{V_m}{RT}\frac{2\gamma_s}{r}\right) \approx C_e\left(1 + \frac{V_m}{RT}\frac{2\gamma_s}{r}\right) \qquad (12)$$

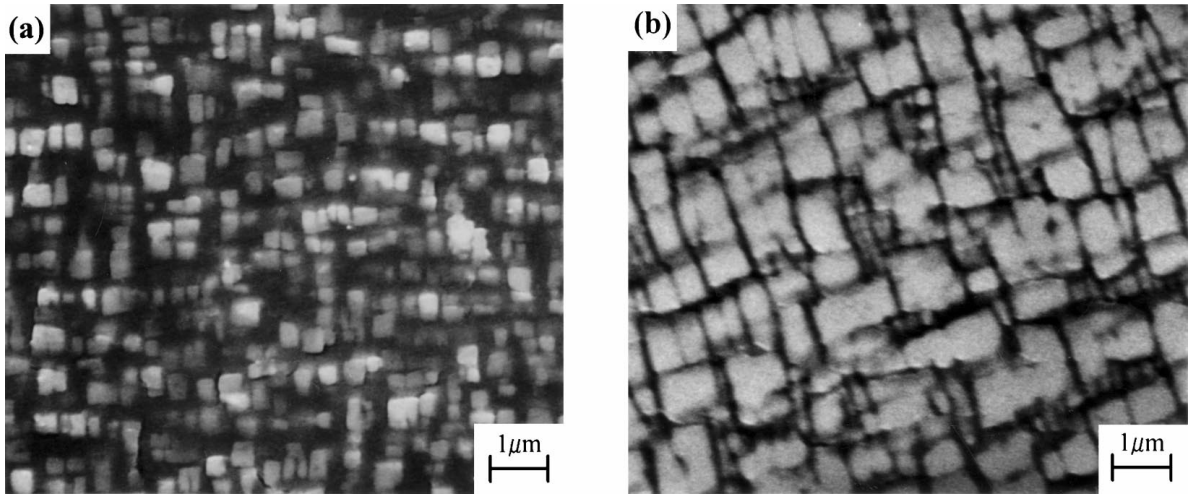

Figure 9 SEM micrograph showing (a) γ' precipitates with the bimodal size distribution after solution treatment at 1210 °C and (b) γ' precipitates with bimodal size distribution after ageing treatment at 950 °C for 48 h.

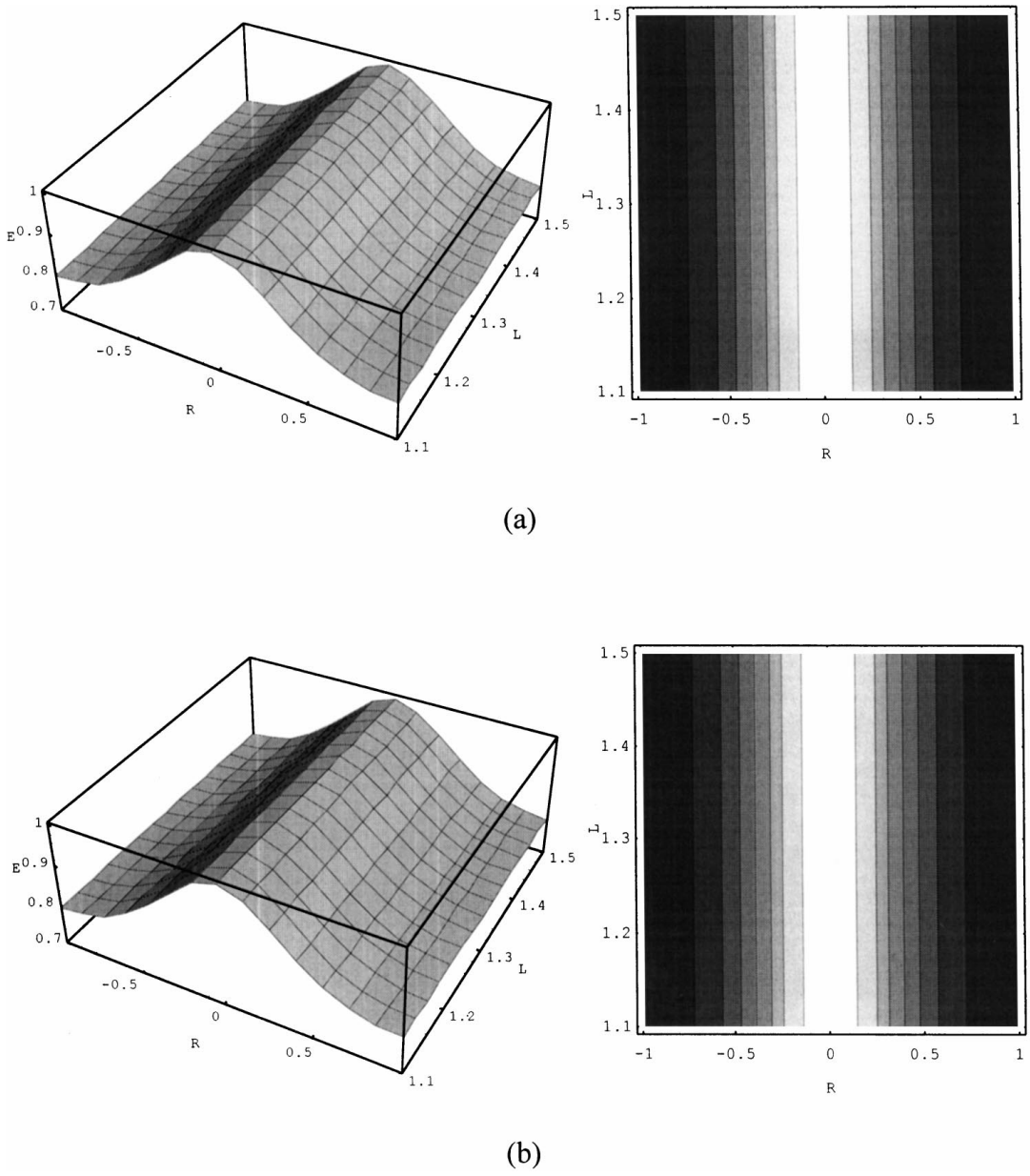

Figure 10 Three-dimensional diagram and contour plot of calculated total energy versus the size parameter, R, and inter-particle spacing, L, when the particles are (a) 0.16 μm and (b) 0.32 μm in diameter without the effect of elastic interaction energy, and when the particles are (c) 0.16 μm and (d) 0.32 μm in diameter with the effect of elastic interaction energy. (*continued)*

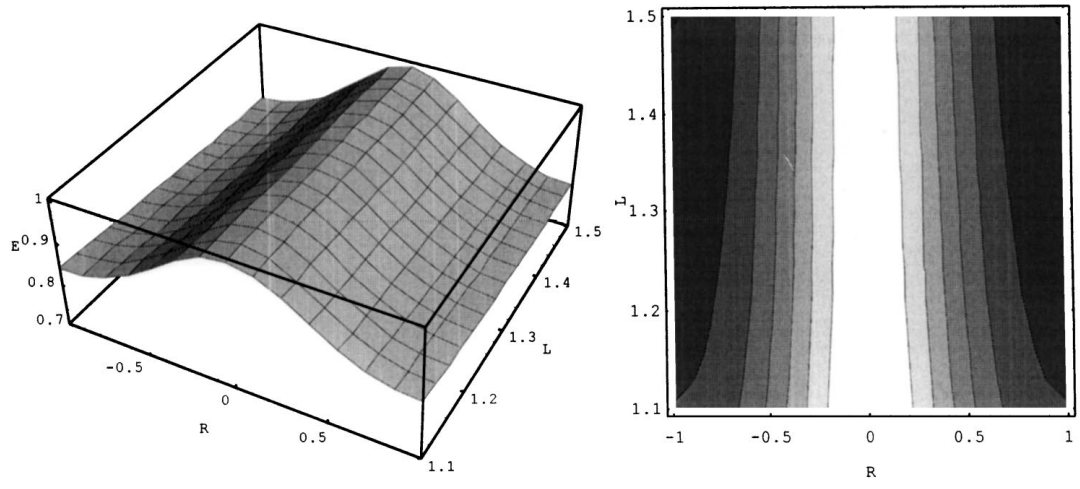

(c)

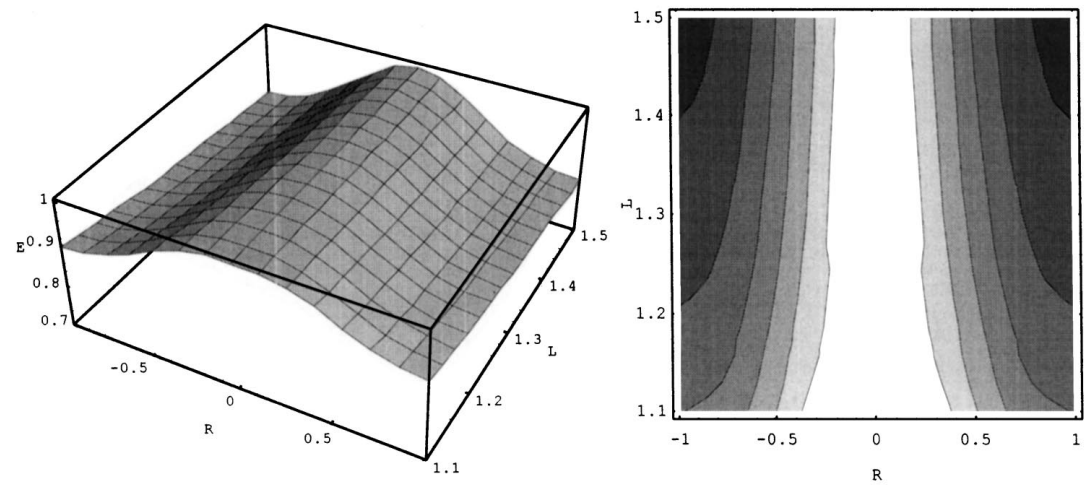

(d)

Figure 10 (*continued)*

When there is no elastic interaction energy, the difference of solubility in particles of radius r is

$$C_r - C_e = \frac{C_e}{RT}\frac{2\gamma_s V_m}{r} = \frac{C_e}{RT}\Delta G_s \qquad (13)$$

When there is an elastic interaction energy, the difference of solubility in particles of radius r is as follows

$$C_r - C_e = \frac{C_e}{RT}\Delta G_i = \frac{C_e}{RT}\left(\frac{2\gamma_s V_m}{r} - BV_m\right) \qquad (14)$$

The difference between Equation 13 and 14 indicates that the elastic interaction energy affects the coarsening rate by changing the solubility of the particle [33, 34].

The growth rate of a particle of radius r is given by,

$$\frac{\mathrm{d}r}{\mathrm{d}t} = \frac{D}{r}(C_m - C_r) \qquad (15)$$

where C_m is the mole fraction of the precipitates component in the matrix. And the exact coarsening rate is calculated from the continuity equation [35]

$$\frac{\partial f(r,t)}{\partial t} + \frac{\partial}{\partial r}\left[f(r,t)\frac{\mathrm{d}r}{\mathrm{d}t}\right] = 0 \qquad (16)$$

where $f(r, t)$ is the distribution function of the precipitate size obtained in the LSW theory [6, 7].

However, the development of the analytical coarsening equation including the effect of the elastic interaction energy needs a more sophisticated model including the size distribution of the precipitates. In this study, the simple two-particle model only explained the gradual decrease of the driving force with increasing particle size when there is an elastic interaction energy. Even when the contribution of the elastic interaction energy is less than the contribution of the interfacial energy, the driving force was found to decrease gradually during the coarsening of the particles. The coarsening rate can

decrease gradually as the precipitates coarsen even in region I in the bifurcation diagram, contrary to previous explanations using the inverse coarsening mechanism [22, 23].

4. Conclusions

The effect of the elastic interaction energy on the coarsening of γ' precipitates in a mechanically alloyed ODS Ni-base superalloy was investigated to explain the gradual deceleration of coarsening of γ' precipitates. The coarsening of γ' precipitates with a bimodal size distribution was typical of Ostwald ripening without showing inverse coarsening behavior. As the contribution of the elastic interaction energy on the total free energy increases with increasing precipitate size, the driving force for the coarsening of γ' precipitates decreases gradually with ageing time.

References

1. C. T. SIMS, N. S. STOLOFF and W. C. HAGEL, in "Superalloys II" (John Wiley & Sons, New York, 1987).
2. J. K. TIEN and T. CAUFIELD, in "Superalloys, Supercomposites and Superceramics" (Academic Press, 1989).
3. A. A. HOPGOOD and J. W. MARTIN, *Mater. Sci. Eng.* **91** (1987) 105.
4. R. A. MACKAY and M. V. NATHAL, *Acta Metall. Mater.* **38** (1990) 993.
5. K. TRINCKAUF, J. PESICKA, C. SCHLESIER and E. NEMBACH, *Phys. Status Solidi A* **131** (1992) 345.
6. I. M. LIFSHITZ and V. V. SLYOZOV, *J. Phys. Chem. Solids* **19** (1961) 35.
7. C. WAGNER, *Z. Electrochem.* **65** (1961) 581.
8. A. J. ARDELL, *Acta Metall.* **20** (1972) 61.
9. P. W. VOORHEES and M. E. GLICKSMAN, *ibid.* **32** (1984) 2001.
10. S. C. HARDY and P. W. VOORHEES, *Metall. Trans. A* **19** (1988) 2713.
11. A. MAHESHWARI and A. J. ARDELL, *Acta Metall. Mater.* **40** (1992) 2661.
12. M. J. KAUFMAN, P. W. VOORHEES, W. C. JOHNSON and F. S. BIANCANIELLO, *Metall. Trans. A* **20** (1989) 2171.
13. A. J. ARDELL, R. B. NICHOLSON and J. D. ESHELBY, *Acta Metall.* **14** (1966) 1295.
14. P. K. FOOTNER and B. P. RICHARDS, *J. Mater Sci.* **17** (1982) 2141.
15. A. ONUKI and H. NISHMORI, *Phys. Rev. B* **43** (1991) 13649.
16. O. PARIS, F. LANGMAYR, G. VOGL and P. FRATZL, *Z. Met.kd.* **86** (1995) 12.
17. A. G. KHACHATURYAN and G. A. SHATALOV, *Sov. Phys.-Solid State* **11** (1969) 118.
18. W. C. JOHNSON and J. K. LEE, *Metall. Trans. A* **10** (1979) 1141.
19. T. A. ABINANDANAN and W. C. JOHNSON, *Acta Metall. Mater.* **41** (1993) 17.
20. T. MIYAZAKI and M. DOI, *Mater. Sci. Eng. A* **110** (1989) 175.
21. K. KAWASAKI and Y. ENOMOTO, *Physica A* **150** (1988) 463.
22. T. MIYAZAKI, T. KOYAMA and M. DOI, *Mater. Sci. Eng. A* **169** (1993) 159.
23. Z. FANG, B. R. PATTERSON and M. E. TURNER, *Acta Metall. Mater.* **40** (1992) 713.
24. W. C. JOHNSON, *Acta Metall.* **32** (1984) 465.
25. J. M. YELLUP and B. A. PARKER, *Phys. Stat. Solidi A* **62** (1980) 637.
26. D. J. CHELLMAN and A. J. ARDELL in Proceedings of the Tenth RISO International Symposium on Metallurgy and Materials Science (1989) p. 295.
27. X. ZHENG, *Z. Phys. B* **93** (1994) 501.
28. A. D. SEQUEIRA, H. A. CALDERON and G. KOSTORZ, *Scr. Metall. Mater.* **30** (1994) 7.
29. H. J. RYU, S. H. HONG and Y. G. KIM, *J. Korean Inst. Met. Mater.* **33** (1995) 1176.
30. H. YAMAUCHI and D. DE FONTAINE, *Acta Metall.* **27** (1979) 763.
31. T. MURA, in "Micromechanics of defects in solids" (Martinus Nijhoff Publishers, 1982).
32. A. J. ARDELL, *Scr. Metall. Mater.* **24** (1990) 343.
33. K. C. KING, P. W. VOORHEES, G. B. OLSON and T. MURA, *Metall. Trans. A* **22** (1991) 2199.
34. T. MIYAZAKI, T. KOYAMA and M. DOI, *Acta Metall. Mater.* **42** (1994) 3417.
35. M. DOI, *Prog. Mater. Sci.* **40** (1996) 79.

Received 28 November 1997
and accepted 19 August 1998